Quaternary Research (2018), **90**, 348–359.

doi:10.1017/qua.2018.33

Using ^{10}Be exposure dating to constrain glacial advances during the late glacial and Holocene on Mount Xuebaoding, eastern Tibetan Plateau

Beibei Liu, Zhijiu Cui, Xu Peng, Yesong Han, Gengnian Liu*
College of Urban and Environmental Sciences, Peking University, Beijing 100871, China

(Received November 9, 2017; Accepted March 9, 2018)

Abstract

Moraines preserved around Mount Xuebaoding (5588 m above sea level) on the eastern margin of the Tibetan Plateau, represent past glacial activity in this area. The chronology of these moraines was established using ^{10}Be exposure dating. The dating results revealed multiple glacial events prior to the late glacial (>14.1 ± 2.2 ka), the late glacial (15.6 ± 1.6 to 11.2 ± 3.0 ka), the early-middle Holocene (9.1 ± 0.9 to 6.7 ± 0.7 ka), and the Neoglacial periods (2.5 ± 0.5 to 1.5 ±0.1 ka). These glacial stages are consistent with the recalculated ages from surrounding areas throughout the Indian and East Asian monsoon-influenced region on the eastern Tibetan Plateau. Comparing with other paleoclimate indexes, we suggest that the late glacial event was mainly driven by low temperature, the early–middle Holocene event by high precipitation, and the late Holocene/Neoglacial event by low temperature.

Keywords: ^{10}Be; Exposure dating; Glaciation; Mount Xuebaoding; Eastern margin of the Tibetan Plateau

INTRODUCTION

The extent of mountain glacier fluctuations may be affected by climate change and local topographic variations (Yi et al., 2008; Davis et al., 2009; Seong et al., 2009; Zhao et al., 2010; Xu et al., 2010). To understand the relationship between glacial change and climate, it is essential to understand the temporal and spatial variability of glaciers in the past. Determining the ages of moraines helps to refine chronologies of glacier fluctuations at key sites and to identify key factors that force the glacial fluctuations. Recently, cosmogenic nuclide exposure dating has been widely used to constrain glacial chronologies in China (Li et al., 2014; Dong et al., 2016; Liu et al., 2017), allowing for the comparison between the timing of glacial advance and climatic change (Zhou et al., 2010; Xu et al., 2013; Li et al., 2016; Zhang et al., 2016a).

This study is focused on Mount Xuebaoding, an area containing distinctive glacial landforms, which have been studied since the 1980s (Luo, 1983; Li et al., 1989; Zheng et al., 1995). Previous studies divided the glacial sequences of this area into four glacial stages based on local names and/or occurrence times (oldest to youngest): the Xuebaoding stage (the penultimate glaciation); the Huanglongsi stage (the last glaciation); the Xuebaoding Neoglaciation; and the Little Ice Age. Shi et al. (2006) also published a map of the glacial landforms in this area. Cao and Guo (2001) used the electron spin resonance method to date glacial tills to 406, 181, 123, and 86 ka in the Sancha and Taojin valleys, but no specific details of the sampling locations nor dating procedures were provided. In this study, we aimed to use ^{10}Be surface exposure dating of moraines to determine the glacial chronology in this area and facilitate a comparison with ages from other regions on the eastern Tibetan Plateau (TP). We focused on two research questions: first, what is the chronology of glacial advances on Mount Xuebaoding; and, second, what mechanisms drove the glacial fluctuations?

REGIONAL SETTING

Mount Xuebaoding, with an altitude of 5588 m above sea level (asl), is the main peak of Min Shan on the eastern margins of the TP (Fig. 1). Five contemporary hanging glaciers are distributed around this peak between 4764 and 5398 m asl, with an area of ~0.84 km^2 (Guo et al., 2014). The lithology of this area is mainly composed of limestone, slate, and sandstone. Three faults control the tectonic movement of this area. Two north-south trending strike-slip thrust faults (the Minjiang and Huya faults) pass along the eastern and western sides of the mountain respectively. Another east-west trending normal fault (the Xueshan Fault) is on the north

*Corresponding author at: College of Urban and Environmental Sciences, Peking University, Beijing 100871, China. E-mail address: liugn@pku.edu.cn (G. Liu).

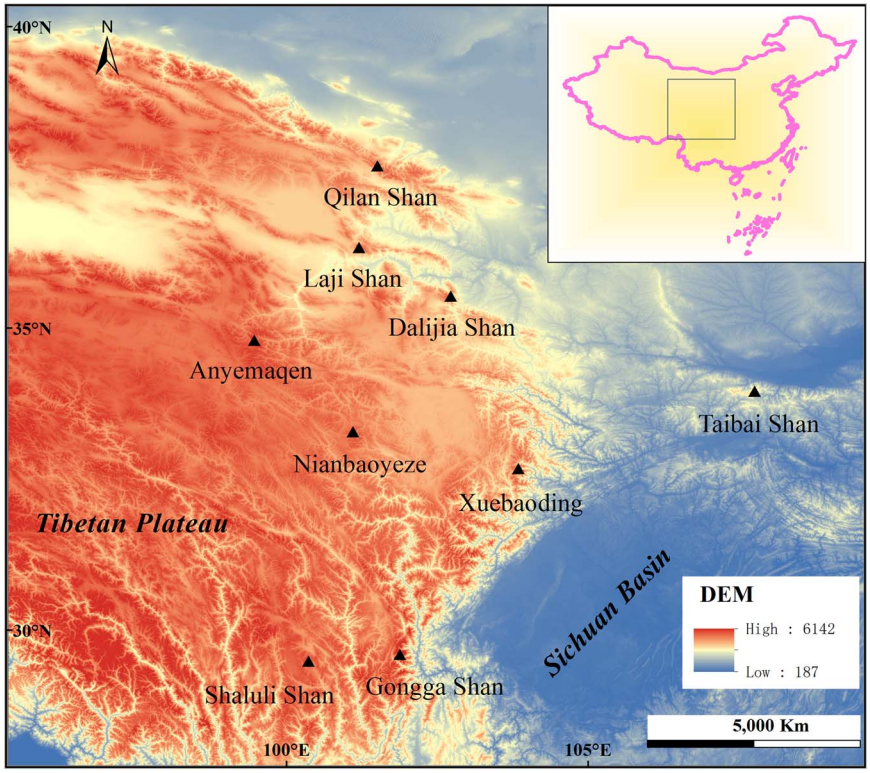

Figure 1. (color online) Digital elevation model (DEM) map of the eastern Tibetan Plateau (TP), showing the location of the Mount Xuebaoding massif and of other mountain ranges in the region which have yielded ^{10}Be ages.

of the massif (Yang et al., 1979; Qian et al., 1995). These three faults are believed to form the Xuebaoding massif.

The nearest meteorological station is the Songpan Station (32.39°N, 103.34°E, 2850 m asl). Records from 1951 to 2007 show that the mean annual temperature and mean annual precipitation were 5.9°C and 718 mm, respectively, and the mean summer temperature reached 13.7°C at this station. This area is located in the climate transition zone between the Indian and East Asian monsoons (Wang et al., 2003) and receives the precipitation from both systems. About 90% of the precipitation falls between April and October (http://data.cma.cn/site/index.html [accessed November 2017]) and falls as snow at high altitudes, leading to a positive glacial mass balance.

Sample sites

We investigated glacial landforms in the Yanjin, Sancha, Rijiu and Nami Valleys. Several sets of moraines were observed within each valley (Figs 2 and 3). No geomorphic evidence suggests that ice advanced beyond the valleys. We sampled nine boulders in the Yanjin Valley, ten boulders in the Sancha Valley and four boulders in the Rijiu Valley for ^{10}Be surface exposure dating (Table 1 and Supplementary Table 1).

The Yanjin Valley is ~4 km long. We identified four major sets of moraines, named from M1 to M4 from the youngest to the oldest. The youngest set of moraines (M1) extends 0.25 km from the valley head to ~4285 m asl. The surface contains meter-sized angular to sub-angular boulders with no significant evidence of weathering. We sampled one boulder from M1. The next set of moraines, M2, is distributed between 4260 and 4210 m asl, about 0.95 km down-valley, and is composed of multiple moraines. We collected three samples from M2: two from boulders and one from quartz pebbles. Frost weathering has broken quartz veins, resulting in quartz pebbles scattered on the ground. The M3 set of moraines is symmetrically distributed downstream from M2, and dissected by fluvial erosion. It extends for ~2.2 km down-valley between 4215and 3950 m asl. We collected five samples from M3. The outermost moraine set, M4, extends ~3.2 km downstream from 3920 to 3780 m asl. It is covered by shrubby vegetation.

The Sancha Valley is ~5 km long and is characterized by extensive and uneven moraines. Based on the relative geomorphic position and the distribution of glacial boulders, we grouped them into four sets comparable with those observed in the Yanjin Valley. We sampled two of the four sets of moraines: M3 and M4. The M1 set of moraines is distributed at 4,300–4,200 m asl; these moraines are characterized by a distinctive rock glacier on their side walls. The M2 set of moraines extends for 2.2 km from the valley head. The M3 set of moraines extends for ~4.2 km from the valley head, with a height of ~20 m above the valley floor. The moraine surfaces are flat and covered with abundant meter-sized boulders. Many boulders have slightly weathered pits. We collected eight samples from M3. An outermost lateral and terminal set of moraines (M4) is preserved at the mountain front from 3720 to 3600 m asl. The moraines exhibit more rounded ridges and are

https://doi.org/10.1017/qua.2018.33 Published online by Cambridge University Press

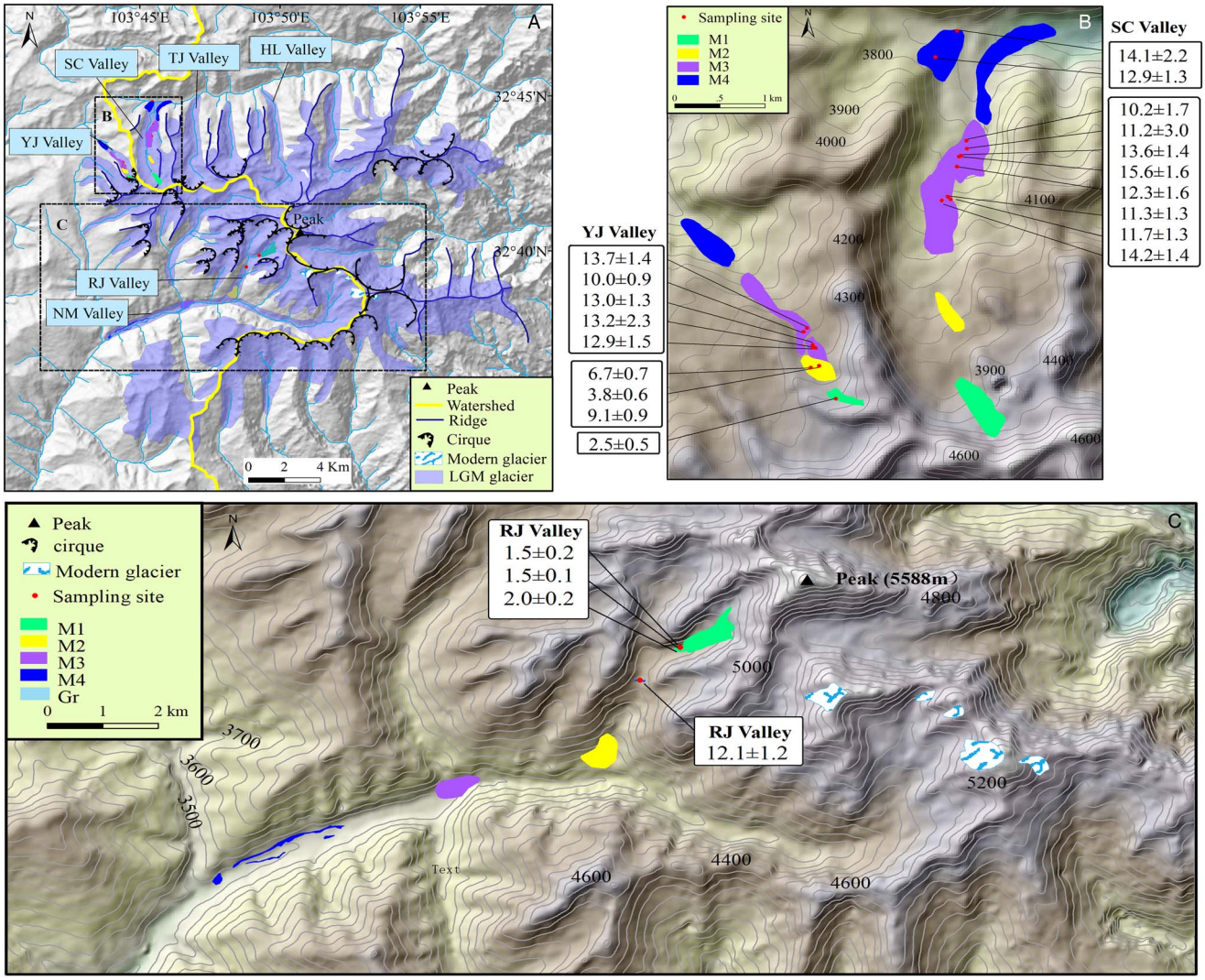

Figure 2. (color online) (A) Digital elevation model (DEM) map of glacier distribution on the Mount Xuebaoding massif as modified by Shi et al. (2006). YJ Valley, Yanjin Valley; SC Valley, Sancha Valley; TJ Valley, Taojin Valley; HL Valley, Huanglong Valley; RJ Valley, Rijiu Valley; and NM Valley, Nami Valley. (B) DEM showing the glacial landforms and sampling sites yielding ^{10}Be data in the Yanjin and Sancha valleys shown in (A). (C) DEM illustrating the glacial landforms and sampling sites recording ^{10}Be data in the Rijiu and Nami valleys shown in (A). All ages are in Ka.

comprised of massive matrix-supported till. They frequently contain heavily pitted and weathered boulders >4 m in diameter, with detritus of weathering evident within each moraine. This set of moraines probably underwent some denudation. We collected two samples from M4.

We identified two groups of moraines in the Rijiu Valley, and two in the Nami Valley, and named them M1, M2, M3 and M4 based on their altitudes, from the highest/youngest (M1) to the lowest/oldest (M4). The Rijiu Valley is a typical U-shaped tributary valley hanging above the main valley. The M1 set of moraines is the youngest in this valley, ranging from 4575 to 4330 m asl. It is defined by a clear glacier tongue covered by seasonal snow, and includes an end moraine with fresh and sharp-crested ridges. The frontal slope of this moraine exhibits a steep gradient of >30°. We sampled three boulders from this moraine for ^{10}Be exposure dating. The moraine set M2 is located from 3900 to 3660 m asl. A rock step (Fig. 2; Gr) exists between M1 and M2 at 4247 m asl. A few glacial boulders lie atop Gr. We collected one sample from the rock step. The moraine set M3 is located at ~3430 m asl, where a tributary valley enters the main (Nami) valley from its northern side. The moraine set M4 consists of two lateral moraines and one end moraine covered with glacially striated boulders. The two lateral moraines are distributed on the two sides of the river between 3340 and 3270 m asl. The end moraine is cut through by the river.

METHODS

Fieldwork and sampling

We conducted geomorphic mapping based on the interpretation of 1:50,000 topographic maps, Google Earth imagery, and

https://doi.org/10.1017/qua.2018.33 Published online by Cambridge University Press

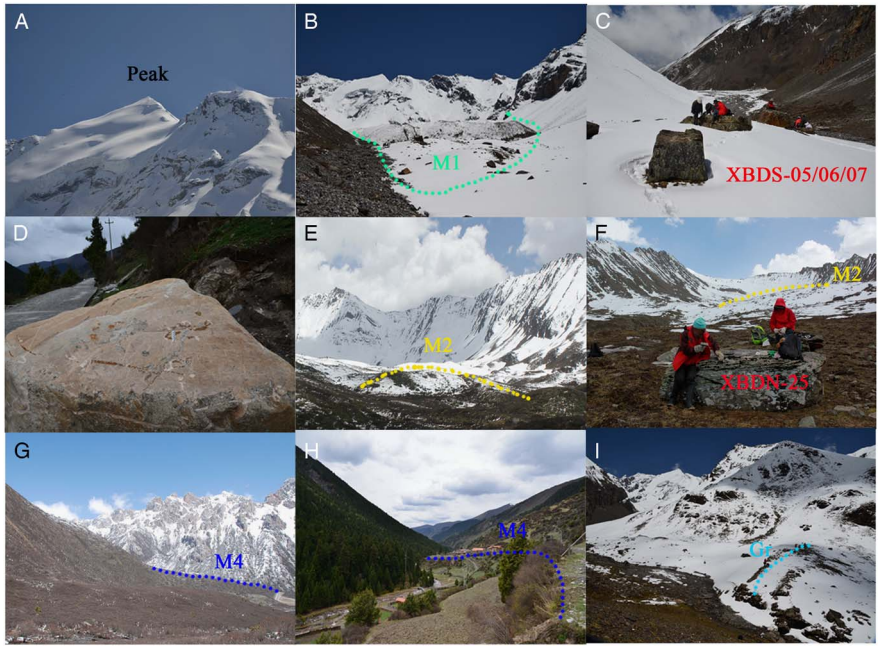

Figure 3. Representative photographs taken in the field. (A) Pyramidal main peak. (B) M1 in the Rijiu Valley (green dashed line showing its extent). (C) Sampled erratic boulders XBDS-05/06/07 on M1 in the Rijiu Valley. (D) Glacially striated boulder in Nami Valley. (E) M2 in the Sancha Valley. (F) M2 in the Yanjin Valley and sampled boulder XBDN-25 on M3 in the same valley. (G) View of the lateral moraine (M4) in the Sancha Valley from upstream (the oldest moraine found). (H) M4 in the Nami Valley, contemporary with M4 in the Yanjin Valley. (I) Rock step (Gr) in the Rijiu Valley, indicating a rapid glacial retreat. (For interpretations of the references to color in this figure legend, the reader is referred to the web version of this article.)

a 30-m ASTER Global Digital Elevation Model (GDEM; http://www.gscloud.cn). The moraine samples were chosen from the flat top surface of large (>1 m) and stable boulders embedded in moraine ridges. Lithologies sampled were generally metamorphic rocks with quartz veins. In total, 23 samples were collected in 2013. We used a handheld GPS unit to determine the latitude, longitude and altitude of the sampled boulders and recorded their lithology and moraine set. We then chiselled off a layer of rock fragments <3 cm thick from the flat surface. We also took photographs of each sample site.

Laboratory methods

Nineteen samples collected from the northern slopes of Mount Xuebaoding were prepared in the Key Laboratory of Tibetan Environment Changes and Land Surface Processes, Institute of Tibetan Plateau Research, Chinese Academy of Sciences. Four samples collected from the southern slopes of the massif were processed at the Institute of Crustal Dynamics, China Seismological Bureau. The physical and chemical analyses follow the modified procedure of Nishiizumi et al. (1984), Kohl and Nishiizumi (1992), and Dortch et al. (2009). The samples were crushed and sieved and the 125–250 μm fraction was used to separate purified quartz. Magnetic separation was used to remove magnetic minerals and then the sample was dissolved in a mixture of concentrated HNO_3 and HCL to eliminate carbonate and organic materials. The sample was repeatedly etched in a dilute solution of HF to dissolve other minerals and remove the outer rim of the quartz crystals. Heavy liquid separation was used to purify the quartz. After cleaning an ICP test was conducted to verify quartz purity. Next, a ^{9}Be carrier of ~0.3 g was added to each purified quartz in a Teflon cup, and dissolved with a HF and HNO_3 solution with heating. After that, a $HClO_4$ solution was added to the Teflon cup for heating to remove the F^- ions. The ^{10}Be separation and purification was achieved using anion and cation ion exchange chromatography. A NH_4OH solution was added into the ^{10}Be for generating $Be(OH)_2$ colloids. Then the $Be(OH)_2$ colloid was oxidized into BeO after dehydration with heating to 750°C for 5 min. The BeO powder mixed with Nb was then loaded in stainless steel targets. Accelerator mass spectrometry (AMS) measurements of the ^{10}Be/^{9}Be were carried out in the Purdue Rare Isotope Measurement Laboratory (PRIME Lab) based on revised TCN ^{10}Be standards (Nishiizumi et al., 2007).

Age calculation and interpretation

We used the CRONUS Earth Version 2.3 online calculator (Balco et al., 2008; Borchers et al., 2016; http://hess.ess.washington.edu/math/) to calculate ^{10}Be exposure ages using different scaling models following the ^{10}Be reference production rate of Heyman (2014), setting the surface erosion rate to zero, the ^{10}Be half time to 1.387 Ma (Chmeleff et al., 2010; Korschinek et al., 2010), and the rock density to 2.7 g/cm^3. Topographic shielding for each sample was calculated using a Python tool and the 30-m ASTER GDEM with designated 5° intervals using both azimuth and altitudinal angles (Li, 2013).

https://doi.org/10.1017/qua.2018.33 Published online by Cambridge University Press

Table 1. Sampling numbers, locations, ^{10}Be concentration, and related parameters and ^{10}Be ages for all samples from Xuebaoding.

Sample name	Relative age	Latitude (°N)	Longitude (°E)	Altitude (m als)	Thickness (cm)	Thickness factor	Shielding correction	^{10}Be concentration (10^3 atoms/g)	Age Time-independent Lal (1991) / Stone (2000) (ka)	Age Desilets et al. (2003,2006) (ka)	Age Dunai (2001) (ka)	Age Lifton et al. (2005) (ka)	Age Time-dependent Lal(1991) / Stone (2000) (ka)
Yanjin Valley													
XBDN-04	M1	32.7042	103.7445	4301	3	0.9751	0.9821	125.82 ± 24.67	2.3 ± 0.5	2.5 ± 0.6	2.7 ± 0.6	2.5 ± 0.6	2.5 ± 0.5
XBDN-18	M2	32.7078	103.7425	4236	3	0.9751	0.9921	195.53 ± 22.15	3.6 ± 0.5	3.8 ± 0.6	4.2 ± 0.7	3.8 ± 0.6	3.8 ± 0.6
XBDN-20	M2	32.7076	103.7415	4236	3	0.9751	0.9943	361.83 ± 21.47	6.7 ± 0.7	6.6 ± 0.9	7.2 ± 0.9	6.6 ± 0.8	6.7 ± 0.7
XBDN-21	M2	32.7078	103.7425	4236	3	1.0000	0.9935	507.12 ± 16.21	9.1 ± 0.8	8.9 ± 1.1	9.5 ± 1.2	8.9 ± 1.0	9.1 ± 0.9
XBDN-22	M3	32.7098	103.7420	4188	3	0.9751	0.9905	683.69 ± 48.16	12.9 ± 1.4	12.5 ± 1.7	13.1 ± 1.8	12.4 ± 1.6	12.9 ± 1.5
XBDN-23	M3	32.7100	103.7417	4180	3	0.9751	0.9905	694.86 ± 104.67	13.2 ± 2.3	12.8 ± 2.5	13.4 ± 2.6	12.6 ± 2.4	13.2 ± 2.3
XBDN-24	M3	32.7101	103.7417	4181	3	0.9751	0.9911	686.47 ± 26.39	13.0 ± 1.2	12.6 ± 1.6	13.2 ± 1.6	12.5 ± 1.5	13.0 ± 1.3
XBDN-25	M3	32.7115	103.7406	4161	3	0.9751	0.9928	523.22 ± 10.53	10.0 ± 0.9	9.8 ± 1.2	10.4 ± 1.2	9.7 ± 1.1	10.0 ± 0.9
XBDN-26	M3	32.7119	103.7410	4154	3	0.9751	0.9922	715.77 ± 25.81	13.8 ± 1.3	13.3 ± 1.7	13.9 ± 1.7	13.1 ± 1.6	13.7 ± 1.4
Sancha Valley													
XBDN-11	M2	32.7262 97	103.7578	3879	3	0.9751	0.9912	528.46 ± 33.77	11.7 ± 1.2	11.6 ± 1.6	12.2 ± 1.6	11.5 ± 1.5	11.7 ± 1.3
XBDN-12	M2	32.7265 58	103.7575	3878	3	0.9751	0.9718	502.42 ± 33.24	11.4 ± 1.2	11.2 ± 1.5	11.8 ± 1.6	11.1 ± 1.4	11.3 ± 1.3
XBDN-15	M2	32.7261 3	103.7567	3877	3	0.9751	0.9906	641.63 ± 21.42	14.2 ± 1.3	14.0 ± 1.7	14.5 ± 1.8	13.8 ± 1.6	14.2 ± 1.4
XBDN-06	M3	32.7327	103.7595	3773	2	0.9833	0.9846	435.13 ± 61.99	10.2 ± 1.7	10.2 ± 1.9	10.8 ± 2.0	10.1 ± 1.8	10.2 ± 1.7
XBDN-07	M3	32.7318 69	103.7596	3787	3	0.9751	0.9856	480.14 ± 119.16	11.2 ± 2.9	11.2 ± 3.1	11.8 ± 3.2	11.1 ± 3.0	11.2 ± 3.0
XBDN-08	M3	32.7310 6	103.7589	3793	2	0.9833	0.9868	593.24 ± 26.81	13.7 ± 1.3	13.5 ± 1.7	14.1 ± 1.8	13.4 ± 1.6	13.6 ± 1.4
XBDN-09	M3	32.7309 1	103.7587	3791	2	0.9833	0.9868	685.30 ± 27.90	15.8 ± 1.5	15.5 ± 2.0	16.0 ± 2.0	15.2 ± 1.8	15.6 ± 1.6
XBDN-10	M3	32.7298 9	103.7585	3807	2	0.9833	0.9862	539.21 ± 49.49	12.4 ± 1.6	12.3 ± 1.9	12.8 ± 1.9	12.1 ± 1.8	12.3 ± 1.6
XBDN-16	M4	32.7418 5	103.7557	3780	3	0.9751	0.9877	551.38 ± 25.63	12.9 ± 1.3	12.8 ± 1.6	13.4 ± 1.7	12.7 ± 1.5	12.9 ± 1.3
XBDN-17	M4	32.7447	103.7583	3741	3	0.9751	0.9911	594.02 ± 72.50	14.2 ± 2.1	14.0 ± 2.4	14.5 ± 2.5	13.8 ± 2.3	14.1 ± 2.2
Rijiu Valley													
XBDS-05	M1	32.66281389	103.8228	4336	2	0.9833	0.9115	75.17 ± 4.07	1.4 ± 0.1	1.5 ± 0.2	1.7 ± 0.2	1.6 ± 0.2	1.5 ± 0.2
XBDS-06	M1	32.66281389	103.8228	4336	2	0.9833	0.9115	76.18 ± 2.45	1.4 ± 0.1	1.6 ± 0.2	1.7 ± 0.2	1.6 ± 0.2	1.5 ± 0.1
XBDS-07	M1	32.66281389	103.8228 72	4336	2.5	0.9792	0.9115	96.50 ± 3.22	1.8 ± 0.2	2.0 ± 0.2	2.2 ± 0.3	2.0 ± 0.2	2.0 ± 0.2
XBDS-11	Gr	32.65651944	103.8152 44	4247	3	0.9751	0.9572	637.26 ± 13.61	12.1 ± 1.1	11.7 ± 1.4	12.3 ± 1.5	11.6 ± 1.3	12.1 ± 1.2

We did not make a correction for shielding due to snow cover, because the seasonal snow cover is sparse at the present-day on the sampling sites and the boulders are too tall to be covered by substantial snow. We assumed the erosion rate as 0 m/Ma. According to Owen et al. (2009), under the erosion rate of 2.5 m/Ma, the exposure ages at about 1 ka should be underestimated by <0.5%, and the ages between 10 and 20 ka should be underestimated by ~2 to 5%. Our interpretations were based on the Lal (1991) and Stone (2000) time-dependent scaling method because it provides convenient comparisons between our data and most of other published data for the region (Fu et al., 2013; Wang et al., 2013; Zhang et al., 2016a).

Both measurement uncertainty and geomorphic processes such as moraine denudation and boulder surface erosion can lead to the scatter of the ages. In terms of geomorphic processes, prior exposure could make the ages much older; where post-depositional degradation could lead to underestimates of the true age (Heyman et al., 2011). We applied a probability density function (PDF) of the measured ages to identify the data cluster or spread (Fig. 4). The potential outliers are identified based on the Chauvent's criterion, which finds a probability band centered on the mean of a normal distribution that should contain all n samples of a data set. By doing this, any data points from the n samples that lie outside this probability band can be considered to be outliers, removed from the data set, and a new mean and standard deviation based on the remaining values and new sample size can be calculated (Chauvenet, 1960; Ross, 2003). Then, we calculated the reduced chi-squared statistic $\left(\chi_R^2\right)$. If the χ_R^2 value was equal to or less than 1.0, it means the ages are clustered and the measurement error is the source of the difference in ages, then the weighed mean age was assumed to represent the moraine age (Barrows et al., 2002; Balco and Schaefer, 2006; Douglass et al., 2006; Balco, 2011; Li et al., 2014; Chen et al., 2015; Li et al., 2016). If the χ_R^2 value was larger than 1.0, it means the ages are scattered and geomorphic processes have resulted in the age scatter; so, we need to use the range of the data to represent the formation time of the moraine set (Li et al., 2014; Chen et al., 2015; Li et al., 2016).

Equilibrium line altitude reconstruction

We used two methods to reconstruct the equilibrium line altitudes (ELAs): the accumulation area ratio (AAR; Meier and Post, 1962) and the terminus-to-headwall altitude ratio (THAR; Benn and Lehmkuhl, 2000) methods. The AAR method assumes that the ratio of the accumulation area and the ablation area of a glacier is a constant value. The THAR method assumes that the ELA must lie between the terminus and the head of the glacier when the glacier is in a steady state condition.

Five modern glaciers occur in our study area. According to Kern and László (2010), the AAR value of 0.44 ± 0.07 is best applied to glaciers with areas in the range of 0.1–1 km^2. We assumed the AAR value is equal to 0.44 and calculated the modern ELA of 5045 m. We adopted 0.5 as the THAR value used to calculate paleo-ELA values (Manley, 1961).

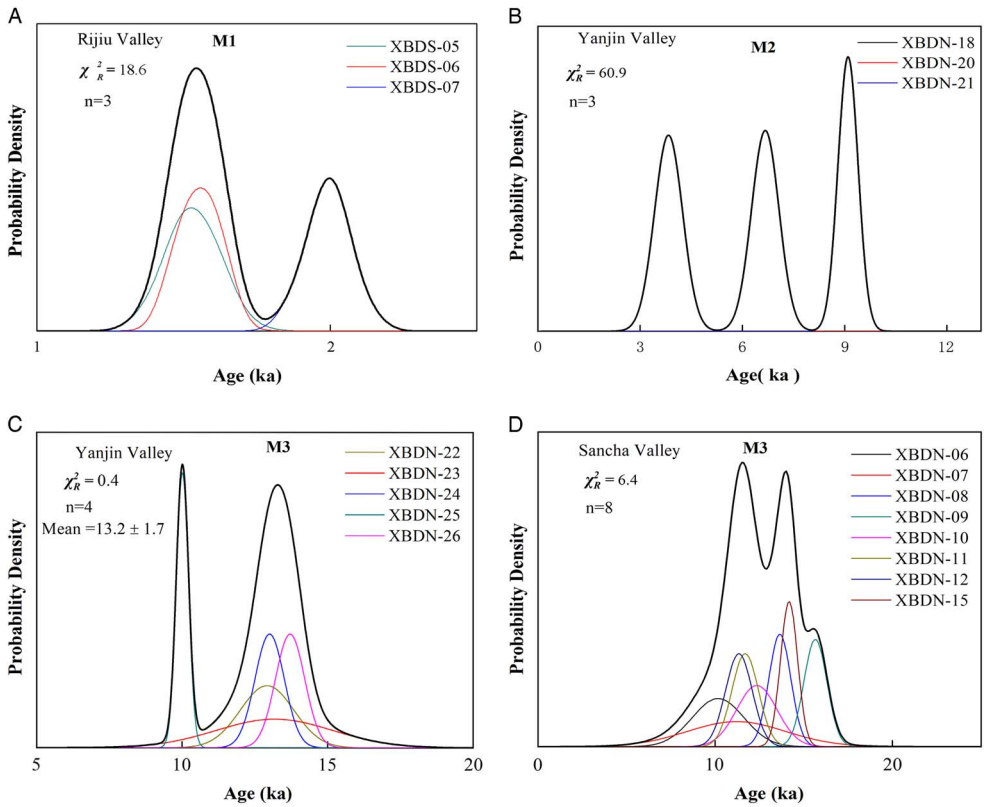

Figure 4. (color online) Probability density function (PDF) plots of ^{10}Be exposure ages for moraines. The χ_R^2 values for moraines are listed in A, B, C and D, and also a mean age is listed in C. (A) M1 in the Rijiu Valley. (B) M2 in the Yanjin Valley. (C) M3 in the Yanjin Valley. (D) M3 in the SanchaValley.

https://doi.org/10.1017/qua.2018.33 Published online by Cambridge University Press

RESULTS

Exposure ages

We obtained 23 ^{10}Be exposure ages from the northern and southern slopes of Mount Xuebaoding.

Yanjin Valley

The age (Sample XBDN-04) obtained from M1 in the Yanjin Valley is 2.5 ± 0.5 ka, indicating a glacial event during the Neoglacial.

The three samples for M2 yield ages of 3.8 ± 0.6, 6.7 ± 0.7 and 9.1 ± 0.9 ka. The PDF of M2 shows a wide exposure age disparity (Fig. 4B). The χ_R^2 value of the three samples on M2 is 60.9 ($P < 0.05$). This indicates that geomorphic processes likely influence the exposure ages. XBDN-18 (3.8 ± 0.6 ka) was sampled from an uneven surface boulder that may be affected by frost shattering, potentially resulting in a significant loss in the cosmogenic nuclide concentration. Therefore, we assign an age range of 9.1 to 6.7 ka to this moraine, indicating a glacial event during the early-middle Holocene.

Five samples (XBDN-22 to -26) taken from M3 in the Yanjin Valley yielded exposure ages of 12.9 ± 1.5, 13.2 ± 2.3, 13.0 ± 1.3, 10.0 ± 0.9, and 13.7 ± 1.4 ka. The PDF (Fig. 4C) did not show a spread of the ages. The Chauvent's criterion, however, identified sample XBDN-25 (10.0 ± 0.9 ka) as an outlier. The lower age than the others may be interpreted as a result of significant post-glacial exhumation. After removing this age, the χ_R^2 value of the remaining four ages is 0.4 ($P > 0.05$), exhibiting a well-developed cluster of ages. Thus, we assign a weighted mean age of 13.2 ± 1.7 ka to this moraine, indicating a glacial event during the late glacial.

Sancha Valley

Eight datasets (samples XBDN-6 to -12, and XBDN-15) from M3 in the Sancha Valley give ^{10}Be ages of 10.2 ± 1.7, 11.2 ± 3.0, 13.6 ± 1.4, 15.6 ± 1.6, 12.3 ± 1.6, 14.2 ± 1.4, 11.3 ± 1.3, and 11.7 ± 1.3 ka, respectively. Neither the PDF plot (Fig. 4D) nor the Chauvent's criterion showed any obvious outliers. The χ_R^2 value of these eight samples is 6.4 ($P < 0.05$), indicating the scatter may be caused by post-depositional degradation or prior exposure. The ^{10}Be exposure age of 10.2 ± 1.7 was sampled from a more strongly weathered surface on the boulder than others, so the age is relatively younger than others. Thus, we assign an age range of 15.6 to 11.2 ka to this moraine, indicating a glacial event during the late glacial.

M4, down-valley from M3, is clearly morpho-stratigraphically older, and was dated to between 14.1 ± 2.2 ka and 12.9 ± 1.3 ka using samples from boulders XBDN-17 and -16, respectively. Because moraine denudation and sample exhumation may underestimate the ages, we assign 14.1 ± 2.2 ka as the minimum exposure age of this moraine, representing a pre-late glacial event.

Rijiu Valley

Three samples (XBDS-5 to -7) collected from M1 in the Rijiu Valley produced ^{10}Be ages of 1.5 ± 0.2, 1.5 ± 0.1 and 2.0 ± 0.2 ka. The PDF (Fig. 4A) of M1 did not show any outlier, nor did Chauvent's criterion. The χ_R^2 value of the three samples on M1 is 18.6 ($P < 0.05$). This implies that geomorphic processes influenced the exposure ages. We used 2.0 to 1.5 ka to represent the age of this moraine set, representing a Neoglacial event. One boulder (XBDS- 11) which lies on bedrock on Gr between M2 and M3, was dated to 12.1 ± 1.2 ka, suggesting a glacial retreat during the late glacial.

Distribution of ELAs

The ELAs for the four dated glacial events are listed in Table 2. The mean ELA of the pre-late glacial is 4084 m asl in the Yanjin Valley (north slope), 4071 m asl in the Sancha Valley (north slope), and 4283 m asl in the Nami Valley (south slope). The altitude of the glacier head in the Nami Valley is higher than the other two valleys, leading to a greater glacial length. The mean ELA of the late glacial is 4175 m asl in the Yanjin Valley, similar to that of 4154 m asl in the Sancha Valley, but lower than the mean ELA of 4343 m asl in the Nami Valley. The mean ELA during the early–middle Holocene varies from 4300 m asl in the Yanjin Valley, 4281 m in the Sancha Valley, to 4503 m asl in the Rijiu Valley. The mean ELA of the Neoglacial changes from 4341 m asl in the Yanjin Valley, 4366 m asl in the Sancha Valley, to a much higher value of 4813 m asl in the Rijiu Valley.

The above results show that the mean ELAs on southern slopes were higher than the values on northern slopes during the different glacial periods. This is likely because southern slopes received more solar radiation and, as a consequence, temperatures on southern/south-facing slopes are often higher, leading to higher ELAs. The geomorphic and ELA

Table 2. Parameters for studied valleys and the calculated equilibrium line altitudes (ELAs) in different periods

Valley	Headwall (m)	Length (km)	ELA (m)			
			Pre-late glacial	Late glacial	Early-middle Holocene	Neoglaciation
Yanjin	4400	4	4084	4175	4300	4341
Sancha	4562	5	4071	4154	4281	4366
Rijiu/Nami	5306	13	4283	4343	4503	4813

https://doi.org/10.1017/qua.2018.33 Published online by Cambridge University Press

evidence shows that glacier coverage in the study area has become restricted since the last glaciation, leading to the increase in the ELA.

The pre-late glacial ELA depression varies from 960 to 974 m on the north slope to 760 m in the south slope. The late glacial ELA depression was 870 to 890 m on the north slope and 700 m on the south slope, respectively. The Holocene ELA depression was between 740 m and 230 m. These results are consistent with the late Pleistocene ELA depression varying between 1000 and 800 m on the eastern TP (Lehmkuhl and Owen, 2005). The ELA depression on Mount Xuebaoding is larger than the mountains in the western part, such as Nianbaoyeze and Anymaqen Shan (ELA depression was ~500 m), corresponding to the decreasing precipitation trend from east to west (Lehmkuhl and Owen, 2005).

DISCUSSION

Glacial history of Mount Xuebaoding

The exposure ages indicate that glaciations were developed much more recently than previously thought in the Xuebaoding massif. Four major glacial events were constrained based on ^{10}Be ages: a pre-late glacial event, a late glacial event, an early–middle Holocene event, and a Neoglacial event. We recalculated the ^{10}Be ages for surrounding mountains (Fig. 1 and 5), using data compiled from previously published literature (Schäfer, 2000; Lasserre et al., 2002; Schäfer et al., 2002; Owen et al., 2003a, 2003b, 2003c, 2005; Graf et al., 2008; Heyman et al., 2011; Fu et al., 2013; Wang et al., 2013; Zhang et al., 2016b), in order to make regional comparisions.

Pre-late glacial event

The pre-late glacial event was prior to 14.1 ka, based on our ^{10}Be exposure ages. The timing of the last glacial maximum (LGM) has been determined for most mountains and massifs on the eastern TP (Lasserre et al., 2002; Schäfer et al., 2002; Owen et al., 2003a, 2003b, 2003c; Graf et al., 2008; Fu et al., 2013; Wang et al., 2013; Zhang et al., 2016b). For example, Lasserre et al. (2002) and Owen et al. (2003c) found that glaciers in the Qilian Mountains appeared to have extended 5–10 km further from their modern positions over a period ranging from 26.5 ± 2.6 to 18.6 ± 2.0 ka. Owen et al. (2003b) also reported that glaciers had advanced between 31.4 ± 3.0 and 17.7 ± 1.7 ka in the Laji Mountains. Two advances (between 22.3 ± 2.2 to 28.8 ± 2.9 ka and 18.8 ± 1.8 to 20.8 ± 2.2 ka) occurred during this time in the Dalijia Mountains (Wang et al., 2013). A set of moraines provided ages ranging from 30.1 ± 2.9 to 15.4 ± 1.5 ka in the Anyemaqen Mountains (Owen et al., 2003a). ^{10}Be ages derived from a rock step on Mount Taibai indicate glacial retreat after 18.3 ± 1.8 ka (Zhang et al., 2016b). At Nianbaoyeze and Ximencuo, glacial stage relics have been dated to between 25.6 ± 2.5 and 18.2 ± 1.9 ka (Owen et al., 2003a). ^{10}Be datasets (between 26.8 ± 2.7 and 17.3 ± 1.8 ka) support the timing of glacial advances in the Shaluli mountain range (Schäfer et al., 2002; Graf et al., 2008; Fu et al., 2013). However, we did not obtain ^{10}Be exposure ages for the LGM in our study area. Perhaps this pre-late glacial event occurred during the LGM or we did not find the glacial relics (glacial landform or boulders) dating to the LGM. The late glacial and Holocene glacial advances may have been more extensive than early events and hence destroyed earlier glacial landforms or sedimentary evidence of earlier glaciations; or, the steeper relief and higher precipitation resulted in more intense landform denudation, leading to the erasure and reworking of older and more extensive glaciations and resulting in extremely poor preservation, only retaining glacial deposits in the central area (Owen et al., 2005, 2008; Schaefer et al., 2008; Stroven et al., 2009).

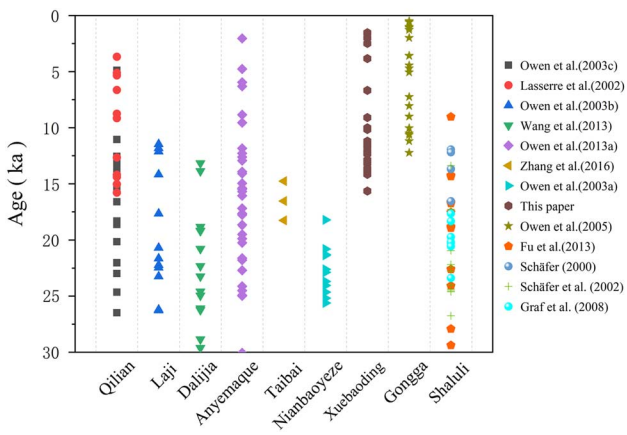

Figure 5. (color online) Comparison of the results of this study with other TCN datasets from the mountains in the eastern Tibetan Plateau shown in Figure 1.

Late glacial event

The late glacial event was dated to 15.6 to 11.2 ka in the Sancha Valley, and 13.7 to 12.9 ka (clustered closely around 13.2 ± 1.7 ka) in Yanjin Valley. The glacial boulder on the rock step appeared to be left by a glacial retreat at 12.1 ± 1.16 ka. This glacial stage has also been identified in the Qilian Mountains ranging from 16.6 ± 1.6 to 11.1 ± 1.1 ka (Lasserre et al., 2002; Owen et al., 2003c). The ^{10}Be ages from the moraines along the northern edge of the Laji Mountains are between 14.2 ± 1.4 and 11.5 ± 1.1 ka, suggesting that one glacial advance occurred during the late glacial (Owen et al., 2003b). Two ages (giving ages of 13.9 ± 1.3 and 13.2 ± 1.3 ka) appear to represent a glacial event during the late glacial in the Dalijia Mountains (Wang et al., 2013). In the Anyemaqen Mountains, the same glacial event has been dated to between 16.1 ± 1.6 and 14.1 ± 1.4 ka (Owen et al., 2003a). In the Gongga Mountains, this episode has been dated to between 12.2 ± 1.3 and 10.0 ± 1.3 ka (Owen et al., 2005), and to between 18.8 ± 1.9 and 11.9 ± 1.5 ka in the Shaluli Mountains (Fu et al., 2013; Schäfer, 2000). Most of the eastern TP mountains experienced this glacial event.

https://doi.org/10.1017/qua.2018.33 Published online by Cambridge University Press

Early-middle Holocene glacial event

It has been reported that multiple glacial advances and retreats took place during the Holocene (Solomina et al., 2015). Our results suggest that a glacial event occurred during the early–middle Holocene, represented by the M2 moraine set within the Yanjin valley. Boulders on moraines in the Anyemaqen Mountains show an age range between 9.6 ± 0.9 and 4.8 ± 0.5 ka (Owen et al., 2003a), and one between 9.0 ± 1.1 and 4.4 ± 0.7 ka in the Gongga Mountains (Owen et al., 2005). So far, only studies of the above three mountain ranges have reported early to middle Holocene glacial advances on the eastern TP.

Neoglacial

Neoglacial events occurred on both the northern and southern slopes of the study area. The ^{10}Be ages were constrained to 2.5 ± 0.5 ka from the Yanjin Valley, and between 2.0 ± 0.2 and 1.5 ± 0.2 ka for the Rijiu Valley. The Neoglacial event also appears to have occurred in the Gongga Mountains, with seven ages from 3.6 ± 1.4 to 1.0 ± 0.5 ka (Owen et al., 2005). The ^{10}Be exposure ages for this glacial event across the eastern TP are scarce.

Driving mechanisms of glacial events

Temperature and precipitation are two major factors affecting glacier change. Figure 6 shows the stalagmite records (Wang et al., 2005; Dutt et al., 2015) and variations in Northern Hemisphere solar radiation as a proxy for changing precipitation and temperature in the region. Ice-core records (Grootes et al., 1993; Thompson et al., 1997) suggest the temperature proxy and provide the link between temperature and glaciation. The YD event is plotted as a proxy for changes in the Northern Hemisphere ice sheets and oceans to assess correlations and connections. The eastern TP and Himalaya are both located in a monsoon-influenced area, and have synchronous glacial advances. Owen et al (2003, 2008) believed glacial events in the eastern TP and Himalaya younger than MIS 2 were dominated by monsoon precipitation rather than by the North Atlantic cooling. Seong et al. (2009) suggested that glacial advances throughout the late glacial and Holocene in the western TP corresponded to rapid climate changes that occurred around the Atlantic Ocean on millennial timescales (Bond et al.,1997). Yi et al. (2008) suggest that the Holocene glacier advances are synchronous with cooling periods identified in the δ^{18}O record in ice cores.

Our ^{10}Be ages from Mount Xuebaoding (Fig. 6A) suggest that glaciers experienced some significant glacial advances during the late glacial. This period was in phase with a pronounced temperature drop in the δ^{18}O ice-core records from Guliya and GISP2 (Fig. 6B and C). In particular, the low temperature during the YD period should have a positive impact on glacial advance. A remarkable total organic content minimum and a rapid grain-size increase at nearby Lake Ximencuo indicate a cold climate, probably in response to the YD event (Zhang and Mischke, 2009). The δ^{13}C values of both mixed peat and mono-species plant cellulose are highest during ~11.8 to 11.2 ka BP at the Hongyuan site near the Xuebaoding massif, suggesting a period of low relative humidity and temperature (Hong et al., 2003). It is therefore hypothesized that low temperatures played a key role in

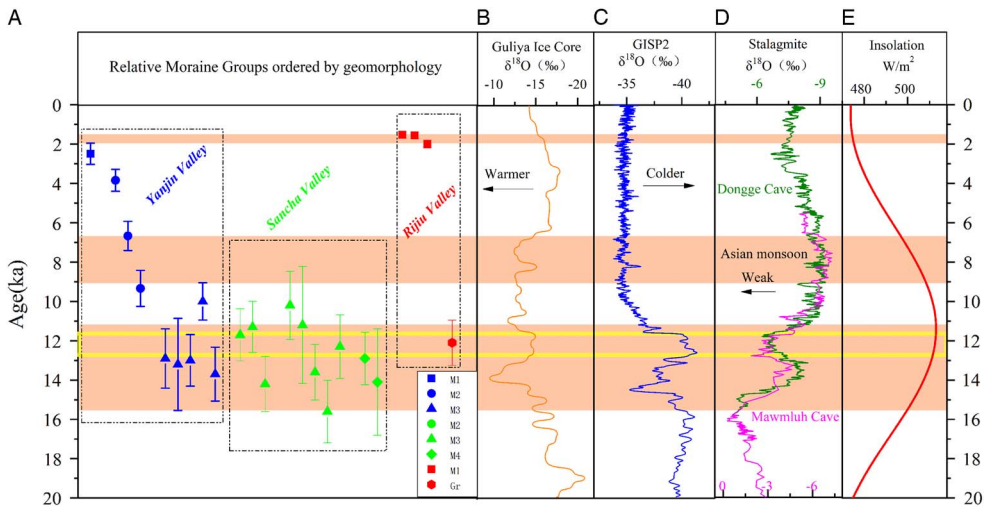

Figure 6. (color online) Multiple proxies for all records. (A) ^{10} Be age with error bar for examples (M1, squares; M2, circles; M3, triangles; M4, diamonds; Gr, hexagons), with Yanjin Valley examples marked in blue, Sancha Valley examples marked in green, and Rijiu Valley examples marked in red. (B) δ^{18}O values for the Guliya Ice Core (Thompson et al., 1997). (C) Greenland Ice Sheet Project Two (GISP2) δ^{18}O values (Grootes et al., 1993). (D) δ^{18}O values for stalagmites from the Dongge and Mawmluh caves (Dutt et al., 2015; Wang et al., 2005). (E) June insolation values at 30°N (Berger and Loutre, 1991). The plots in the black dashed rectangles belong to the same valleys (labeled). The δ^{18}O scales are reversed in the Guliya and Greenland ice cores (increasing leftward) compared with the stalagmites of the Dongge and Mawmluh caves (increasing rightward). The pink bars denote the timing of glacial advances on the Mount Xuebaoding massif. The yellow rectangle denotes the YD event. (For interpretations of the references to color in this figure legend, the reader is referred to the web version of this article.)

https://doi.org/10.1017/qua.2018.33 Published online by Cambridge University Press

controlling glacial advances during the late glacial, as suggested by Hu et al. (2016) from other environmental indices. Increased insolation (Fig. 6E) led to a strong monsoon (Fig. 6D) during the early–middle Holocene. Abundant precipitation fell as snow at high altitudes, which led to positive glacial mass balance and glacial advance. The peat $\delta^{13}C$ time series from Hongyuan suggests a high humidity and high temperature during the early-middle Holocene (Hong et al., 2003). As a result, precipitation is believed to be fundamental in controlling glaciation in these regions during the early-middle Holocene. In the late Holocene/Neoglacial, although precipitation would have been reduced during the insolation minima, the temperature was low enough to lead to positive glacier mass balance, allowing glacier advance. The Guliya Ice core indicates cool temperatures during the Neoglacial period (Fig. 6B). Solar insolation at 30ºN was lower during this period (Fig. 6E; Berger and Loutre, 1991), and the Dongge Cave record shows weak Asian Monsoon events around 4.4, 2.7 and 1.6 ka (Fig. 6C; Wang et al., 2005), indicating lower rainfall during these phases. Study of the peat record of the eastern TP has shown a strengthening Asian Winter Monsoonal (AWM) and a weakening Asian Summer Monsoonal (ASM) since ~4.2 ka, reflecting a cold and dry environment (Yu et al., 2006). It seems that low temperatures were the dominant driving factor behind any Neoglacial glacial advances (Ou et al.,2014).

CONCLUSIONS

We obtained 23 ^{10}Be exposure ages for three valleys in Mount Xuebaoding area. These ages suggest at least four glacial events in this area: prior to the late glacial, during the late glacial, early–middle Holocene, and Neoglacial periods. The mean ELAs on southern slopes were higher than the values on northern slopes during different periods because of higher solar radiation and temperatures on the southern slope. The ELA depression on Mount Xuebaoding is larger than the mountains in the western part of the TP, corresponding to the decreasing precipitation trend from east to west. The glacial chronology of Mount Xuebaoding is synchronous with that of other mountain ranges, despite slight differences in the timing and extent. In summary, glacial advances during the late glacial was most likely driven by the low temperature; the early-middle Holocene glacial advance was mainly controlled by precipitation; and the late Holocene/Neoglacial glacial event is also related to a cooling environment.

ACKNOWLEDGMENTS

This work was supported by the National Natural Science Foundation of China (Grant Nos. 41230743, 41771005, 41671005, and 41371082). We thank Jiafu Zhang, Wei Zhang, Jingdong Zhao, Jie Wang, Xiufeng Yin, and Zhenyu Nie for their help in the field investigation. We thank Chaolu Yi and Jinhua Liu at the Key Laboratory of Tibetan Environment Changes and Land Surface Processes, Institute of Tibetan Plateau Research, Chinese Academy of Sciences for their help in sample preparation. We appreciate Dr. Jackson S. George and Thomas E. Woodruff at the PRIME Lab for sample measurements and Dr. Edward Derbyshire for manuscript editing. We thank the reviewers and editors for their constructive comments.

SUPPLEMENTARY MATERIAL

To view supplementary material for this article, please visit https://doi.org/10.1017/qua.2018.33

REFERENCES

Balco, G., 2011. Contributions and unrealized potential contributions of cosmogenic-nuclide exposure dating to glacier chronology, 1990–2010. *Quaternary Science Reviews* 30, 3–27.

Balco, G., Schaefer, J.M., 2006. Cosmogenic-nuclide and varve chronologies for the deglaciation of southern New England. *Quaternary Geochronology* 1, 15–28.

Barrows, T.T., Stone, J.O., Fifield, L.K., Cresswell, R.G., 2002. The timing of the last glacial maximum in Australia. *Quaternary Science Reviews* 21, 159–173.

Balco, G., Stone, J.O., Lifton, N.A., Dunai, T.J., 2008. A complete and easily accessible means of calculating surface exposure ages or erosion rates from ^{10}Be and ^{26}Al measurements. *Quaternary Geochronology* 3, 174–195.

Benn, D.I., Lehmkuhl, F., 2000. Mass balance and equilibrium-line altitudes of glaciers in high-mountain environments. *Quaternary International* 65, 15–29.

Berger, A., Loutre, M.F., 1991. Insoulation values for the climate of the last 10 million years. *Quaternary Science Reviews* 10, 297–317.

Bond, G., Showers, W., Cheseby, M., Lotti, R., Almasi, P., Priore, P., Cullen, H., Hajdas, I., Bonani, G., 1997. A pervasive millennial-scale cycle in North Atlantic Holocene and glacial climates. *Science* 278, 1257–1266.

Borchers, B., Marrero, S., Balco, G., Caffee, M., Goehring, B., Lifton, N., Nishiizumi, K., Phillips, F., Schaefer, J., Stone, J., 2016. Geological calibration of spallation production rates in the CRONUS-Earth project. *Quaternary Geochronology* 31, 188–198.

Cao, J., Guo, J., 2001. Quaternary ice age division and paleoclimate and paleoenvironment in the Huanglong Nature Reserve, Songpan. *Acta Geologica Sichuan* 21, 141–146.

Chauvenet, W., 1960. *A Manual of Spherical and Practical Astronomy*. 5th ed., 2 vols. Dover Publication, New York.

Chen, Y., Li, Y., Wang, Y., Zhang, M., Cui, Z., Yi, C., Liu, G., 2015. Late Quaternary glacial history of the Karlik Range, easternmost Tian Shan, derived from ^{10}Be surface exposure and optically stimulated luminescence datings. *Quaternary Science Reviews* 115, 17–27.

Chmeleff, J., von Blanckenburg, F., Kossert, K., Jakob, D., 2010. Determination of the ^{10}Be half-life by multicollector ICP-MS and liquid scintillation counting. *Nuclear Instruments and Methods in Physics Research Section B: Beam Interactions with Materials and Atoms* 268, 192–199.

Davis, P.T., Menounos, B., Osborn, G., 2009. Holocene and latest Pleistocene alpine glacier fluctuations: a global perspective. *Quaternary Science Reviews* 28, 2021–2033.

Dong, G., Huang, F., Yi, C., Liu, X., Zhou, W., Caffee, M.W., 2016. Mid-late Pleistocene glacial evolution in the Grove Mountains, East Antarctica, constraints from cosmogenic ^{10}Be surface exposure dating of glacial erratic cobbles. *Quaternary Science Reviews* 145, 71–81.

Dortch, J.M., Owen, L.A., Haneberg, W.C., Caffee, M.W., Dietsch, C., Kamp, U., 2009. Nature and timing of large landslides in the Himalaya and Transhimalaya of northern India. *Quaternary Science Reviews* 28, 1037–1054.

Douglass, D., Singer, B., Kaplan, M., Mickelson, D., Caffee, M., 2006. Cosmogenic nuclide surface exposure dating of boulders on last-glacial and late-glacial moraines, Lago Buenos Aires, Argentina: interpretive strategies and paleoclimate implications. *Quaternary Geochronology* 1, 43–58.

Dutt, S., Gupta, A.K., Clemens, S.C., Cheng, H., Singh, R.K., Kathayat, G., Edwards, R.L., 2015. Abrupt changes in Indian summer monsoon strength during 33,800 to 5500 years BP. *Geophysical Research Letters* 42, 5526–5532.

Fu, P., Stroeven, A.P., Harbor, J.M., Hättestrand, C., Heyman, J., Caffee, M.W., Zhou, L., 2013. Paleoglaciation of Shaluli Shan, southeastern Tibetan Plateau. *Quaternary Science Reviews* 64, 121–135.

Graf, A., Strasky, S., Zhao, Z., Akçar, N., Ivy-Ochs, S., Kubik, P., Christl, M., Kasper, H., Wieler, R., Schlüchter, C., 2008. *Glacier Extension on the Eastern Tibetan Plateau in Response to MIS 2 Cooling, With a Contribution to ^{10}Be and ^{21}Ne Methodology Glacial Response To Global Climate Changes: Cosmogenic Nuclide Chronologies from High and Low Latitudes*. PhD dissertation, University of Bern, Bern, Switzerland.

Grootes, P., Stuiver, M., White, J., Johnsen, S., Jouzel, J., 1993. Comparison of oxygen isotope records from the GISP2 and GRIP Greenland ice cores. *Nature* 366, 552–554.

Guo, W., Xu, J., Liu, S., Shangguan, D., Wu, L., Yao, X., Zhao, J., Liu, Q., Jiang, Z., Li, P., 2014. The second glacier inventory dataset of China (version 1.0). Cold and Arid Regions Science Data Center, Lanzhou, China. http://dx.doi.org/10.3972/glacier.001.2013.db.

Heyman, J., 2014. Paleoglaciation of the Tibetan Plateau and surrounding mountains based on exposure ages and ELA depression estimates. *Quaternary Science Reviews* 91, 30–41.

Heyman, J., Stroeven, A.P., Harbor, J.M., Caffee, M.W., 2011. Too young or too old: evaluating cosmogenic exposure dating based on an analysis of compiled boulder exposure ages. *Earth and Planetary Science Letters* 302, 71–80.

Hong, Y., Hong, B., Lin, Q., Zhu, Y., Shibata, Y., Hirota, M., Uchida, M., Leng, X., Jiang, H., Xu, H., 2003. Correlation between Indian Ocean summer monsoon and North Atlantic climate during the Holocene. *Earth and Planetary Science Letters* 211, 371–380.

Hu, G., Yi, C.-L., Zhang, J.-F., Liu, J.-H., Jiang, T., Li, S.-H., 2016. Late Quaternary glacial advances in the eastern Qilianshan, northeastern Tibet, as inferred from luminescence dating of fluvioglacial sediments. *Journal of Quaternary Science* 31, 587–597.

Kern, Z., László, P., 2010. Size specific steady-state accumulation-area ratio: an improvement for equilibrium-line estimation of small palaeoglaciers. *Quaternary Science Reviews* 29, 2781–2787.

Kohl, C., Nishiizumi, K., 1992. Chemical isolation of quartz for measurement of in-situ-produced cosmogenic nuclides. *Geochimica et Cosmochimica Acta* 56, 3583–3587.

Korschinek, G., Bergmaier, A., Faestermann, T., Gerstmann, U., Knie, K., Rugel, G., Wallner, A., Dillmann, I., Dollinger, G., Von Gostomski, C.L., 2010. A new value for the half-life of ^{10}Be by heavy-ion elastic recoil detection and liquid scintillation counting. *Nuclear Instruments and Methods in Physics Research Section B: Beam Interactions with Materials and Atoms* 268, 187–191.

Lal, D., 1991. Cosmic ray labeling of erosion surfaces: in situ nuclide production rates and erosion models. *Earth and Planetary Science Letters* 104, 424–439.

Lasserre, C., Gaudemer, Y., Tapponnier, P., Mériaux, A.S., Van der Woerd, J., Daoyang, Y., Ryerson, F.J., Finkel, R.C., Caffee, M.W., 2002. Fast late Pleistocene slip rate on the Leng Long Ling segment of the Haiyuan fault, Qinghai, China. *Journal of Geophysical Research: Solid Earth* 107, 2276–2291.

Lehmkuhl, F., Owen, L.A., 2005. Late Quaternary glaciation of Tibet and the bordering mountains: a review. *Boreas* 34, 87–100.

Li, Y., 2013. Determining topographic shielding from digital elevation models for cosmogenic nuclide analysis: a GIS approach and field validation. *Journal of Mountain Science* 10, 355–362.

Li, Y., Li, Y., Harbor, J., Liu, G., Yi, C., Caffee, M.W., 2016. Cosmogenic ^{10}Be constraints on Little Ice Age glacial advances in the eastern Tian Shan, China. *Quaternary Science Reviews* 138, 105–118.

Li, Y., Liu, G., Chen, Y., Li, Y., Harbor, J., Stroeven, A.P., Caffee, M., Zhang, M., Li, C., Cui, Z., 2014. Timing and extent of Quaternary glaciations in the Tianger Range, eastern Tian Shan, China, investigated using ^{10}Be surface exposure dating. *Quaternary Science Reviews* 98, 7–23.

Li, Z., Wang, M., Chen, Z., 1989. Discussion on divide and comparison of Quaternary glacial periods in western China. In: Gao, S., Zheng, Y. (Eds.), *Hengduan Mountains Studies*. Sichuan Science and Technology Publishing House, Sichuan, China, pp. 37–49.

Liu, J., Yi, C., Li, Y., Bi, W., Zhang, Q., Hu, G., 2017. Glacial fluctuations around the Karola Pass, eastern Lhagoi Kangri Range, since the Last Glacial Maximum. *Journal of Quaternary Science* 32, 516–527.

Luo, L., 1983. The summit of the Min mountain range-Xuebaoding. *Journal of the Southwest Teachers College* 27, 131–140.

Manley, G., 1961. The late-glacial climate of north-west England. *Geological Journal* 2, 188–215.

Meier, M.F., Post, A., 1962. Recent variations in mass net budgets of glaciers in western North America. *International Association of Hydrological Sciences Publication* 58, 63–77.

Nishiizumi, K., Elmore, D., Ma, X., Arnold, J., 1984. ^{10}Be and ^{36}Cl depth profiles in an Apollo 15 drill core. *Earth and Planetary Science Letters* 70, 157–163.

Nishiizumi, K., Imamura, M., Caffee, M.W., Southon, J.R., Finkel, R.C., McAninch, J., 2007. Absolute calibration of ^{10}Be AMS standards. *Nuclear Instruments and Methods in Physics Research Section B: Beam Interactions with Materials and Atoms* 258, 403–413.

Ou, X., Lai, Z., Zhou, S., Zeng, L., 2014. Timing of glacier fluctuations and trigger mechanisms in eastern Qinghai–Tibetan Plateau during the late Quaternary. *Quaternary Research* 81, 464–475.

Owen, L.A., Caffee, M.W., Finkel, R.C., Seong, Y.B., 2008. Quaternary glaciation of the Himalayan–Tibetan orogen. *Journal of Quaternary Science* 23, 513–531.

Owen, L.A., Finkel, R.C., Barnard, P.L., Haizhou, M., Asahi, K., Caffee, M.W., Derbyshire, E., 2005. Climatic and topographic controls on the style and timing of Late Quaternary glaciation throughout Tibet and the Himalaya defined by ^{10}Be cosmogenic radionuclide surface exposure dating. *Quaternary Science Reviews* 24, 1391–1411.

Owen, L.A., Finkel, R.C., Haizhou, M., Spencer, J.Q., Derbyshire, E., Barnard, P.L., Caffee, M.W., 2003a. Timing and style of Late Quaternary glaciation in northeastern Tibet. *Geological Society of America* 115, 1356–1364.

Owen, L.A., Ma, H., Derbyshire, E., Spencer, J.Q., Barnard, P.L., Zeng, Y.N., Finkel, R., Caffee, M., 2003b. The timing and style of Late Quaternary glaciation in the La Ji Mountains, NE Tibet: evidence for restricted glaciation during the latter part of the Last Glacial. *Zeitschrift für Geomorphologie* 130, 263–276.

Owen, L.A., Robinson, R., Benn, D.I., Finkel, R.C., Davis, N.K., Yi, C., Putkonen, J., Li, D., Murray, A.S., 2009. Quaternary glaciation of Mount Everest. *Quaternary Science Reviews* 28, 1412–1433.

Owen, L.A., Spencer, J.Q., Haizhou, M.A., Barnard, P.L., Derbyshire, E., Finkel, R.C., Caffee, M.W., Nian, Z.Y., 2003c. Timing of Late Quaternary glaciation along the southwestern slopes of the Qilian Shan, Tibet. *Boreas* 32, 281–291.

Qian, H., Ma, S., Gong, Y., 1995. Discussions on the Minjiang Fault. *Earthquake Research in China* 11, 140–146.

Ross, S.M., 2003. Peirce's criterion for the elimination of suspect experimental data. *Journal of Engineering Technology* 20, 38–41.

Schäfer, J.M., 2000. Reconstruction of landscape evolution and continental paleoglaciations using in-situ cosmogenic nuclides.

Schaefer, J.M., Oberholzer, P., Zhao, Z., Ivy-Ochs, S., Wieler, R., Baur, H., Kubik, P.W., Schlüchter, C., 2008. Cosmogenic beryllium-10 and neon-21 dating of late Pleistocene glaciations in Nyalam, monsoonal Himalayas. *Quaternary Science Reviews* 27, 295–311.

Schäfer, J.M., Tschudi, S., Zhao, Z., Wu, X., Ivy-Ochs, S., Wieler, R., Baur, H., Kubik, P.W., Schlüchter, C., 2002. The limited influence of glaciations in Tibet on global climate over the past 170 000 yr. *Earth and Planetary Science Letters* 194, 287–297.

Seong, Y.B., Owen, L.A., Yi, C., Finkel, R.C., 2009. Quaternary glaciation of Muztag Ata and Kongur Shan: Evidence for glacier response to rapid climate changes throughout the Late Glacial and Holocene in westernmost Tibet. *Geological Society of America Bulletin* 121, 348–365.

Shi, Y., Cui, Z., Su, Z., 2006. *Glaciations and Envitonmental Variations in China*. Hebei Science and Tecnology Press, Hebei.

Solomina, O.N., Bradley, R.S., Hodgson, D.A., Ivy-Ochs, S., Jomelli, V., Mackintosh, A.N., Nesje, A., Owen, L.A., Wanner, H., Wiles, G.C., Young, N.E., 2015. Holocene glacier fluctuations. *Quaternary Science Reviews* 111, 9–34.

Stone, J.O., 2000. Air pressure and cosmogenic isotope production. *Journal of Geophysical Research: Solid Earth* 105, 23753–23759.

Stroeven, A., Hättestrand, C., Heyman, J., Harbor, J., Li, Y., Zhou, L., Caffee, M., Alexanderson, H., Kleman, J., Ma, H., 2009. Landscape analysis of the Huang He headwaters, NE Tibetan Plateau—Patterns of glacial and fluvial erosion. *Geomorphology* 103, 212–226.

Thompson, L.O., Yao, T., Davis, M., Henderson, K., Mosley-Thompson, E., Lin, P.-N., Beer, J., Synal, H.-A., Cole-Dai, J., Bolzan, J., 1997. Tropical climate instability: The last glacial cycle from a Qinghai-Tibetan ice core. *Science* 276, 1821–1825.

Wang, B., Clemens, S.C., Liu, P., 2003. Contrasting the Indian and East Asian monsoons: implications on geologic timescales. *Marine Geology* 201, 5–21.

Wang, J., Kassab, C., Harbor, J.M., Caffee, M.W., Cui, H., Zhang, G., 2013. Cosmogenic nuclide constraints on late Quaternary glacial chronology on the Dalijia Shan, northeastern Tibetan Plateau. *Quaternary Research* 79, 439–451.

Wang, Y., Cheng, H., Lawrence Edwards, R., He, Y., Kong, X., An, Z., Wu, J., Kelly, M.J., Dykoski, C.A., Li, X., 2005. The Holocene Asian Monsoon: Links to Solar Changes and North Atlantic Climate. *Science* 308, 854–857.

Xu, L., Ou, X., Lai, Z., Zhou, S., Wang, J., Fu, Y., 2010. Timing and style of Late Pleistocene glaciation in the Queer Shan, northern Hengduan Mountains in the eastern Tibetan Plateau. *Journal of Quaternary Science* 25, 957–966.

Xu, X., Hu, G., Qiao, B., 2013. Last glacial maximum climate based on cosmogenic ^{10}Be exposure ages and glacier modeling for the head of Tashkurgan Valley, northwest Tibetan Plateau. *Quaternary Science Reviews* 80, 91–101.

Yang, J., Deng, T., Wang, Y., Wen, X., 1979. The Quaternary tectonic stress states over the upstream area of Minjiang River in Sichuan and its relations to earthquakes. *Seismology and Geology* 1, 68–75.

Yi, C., Chen, H., Yang, J., Liu, B., Fu, P., Liu, K., Li, S., 2008. Review of Holocene glacial chronologies based on radiocarbon dating in Tibet and its surrounding mountains. *Journal of Quaternary Science* 23, 533–543.

Yu, X., Zhou, W., Franzen, L.G., Xian, F., Cheng, P., Jull, A.T., 2006. High-resolution peat records for Holocene monsoon history in the eastern Tibetan Plateau. *Science in China Series D* 49, 615–621.

Zhang, C., Mischke, S., 2009. A Late glacial and Holocene lake record from the Nianbaoyeze Mountains and inferences of lake, glacier and climate evolution on the eastern Tibetan Plateau. *Quaternary Science Reviews* 28, 1970–1983.

Zhang, M., Chen, Y., Li, Y., Liu, G., 2016a. Late Quaternary glacial history of the Nalati Range, central Tian Shan, China, investigated using ^{10}Be surface exposure dating. *Journal of Quaternary Science* 31, 659–670.

Zhang, W., Liu, L., Chen, Y., Liu, B., Harbor, J.M., Cui, Z., Liu, R., Liu, X., Zhao, X., 2016b. Late glacial ^{10}Be ages for glacial landforms in the upper region of the Taibai glaciation in the Qinling Mountain range, China. *Journal of Asian Earth Sciences* 115, 383–392.

Zhao, J., Song, Y., King, J.W., Liu, S., Wang, J., Wu, M., 2010. Glacial geomorphology and glacial history of the Muzart River valley, Tianshan range, China. *Quaternary Science Reviews* 29, 1453–1463.

Zheng, B., Li, S., Wang, S., 1995. Evolution of Quaternary glacier on the surrounding mountains of the Zoige Basin. In, *Tibetan Project Expert Committee (Eds.), Formation of Environmental Change and the Evolution of the Qinghai-Tibet Plateau Ecological System (Annual Academic Papers)*. Science Press, Beijing, pp. 218–226.

Zhou, S., Z., Wang, J., Xu, L., Wang, X., L., Colgan, P.M., Mickelson, D.M., 2010. Glacial advances in southeastern Tibet during late Quaternary and their implications for climatic changes. *Quaternary International* 218, 58–66.

https://doi.org/10.1017/qua.2018.33 Published online by Cambridge University Press